

Supporting Information

S1 Kinetics experiment – Visual determination of nanoparticle formation by color change

An experiment was performed as a proof-of-concept for the method of visual inspection of color change as a qualitative means to evaluate the formation and growth of nanoparticles during the reaction progress. A synthesis was carried out at 195 °C where 0.10 mmol Pt(acac)₂ and 2.0 mmol of PVP was reacted in 20 mL EG, identical to the reaction kinetics experiment in the main manuscript. During the progress of the reaction, small volumes of the reaction mixture were withdrawn for visual inspection of color at the respective time point (Fig. S1-1) analogous to the main manuscript, and these samples were characterized by high-resolution SEM. Note that the color of the reaction mixture annotated by (*) refers to the homogenization step where Pt(acac)₂ and PVP is dissolved in EG at 100 °C. At time point 0 just after reaching 195 °C and beyond, the color becomes gradually darker until it is dark brown after 50 minutes.

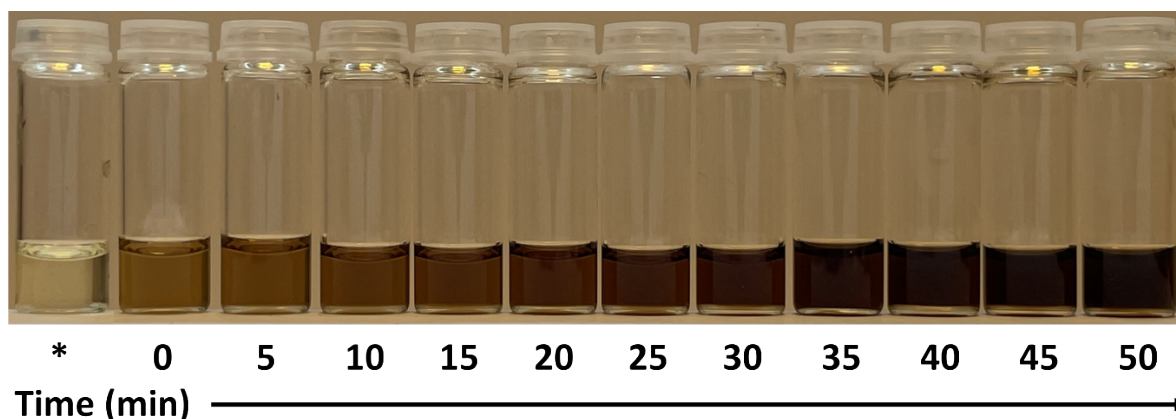


Fig. S1-1 The color change in the reaction mixture as a function of time after 195 °C is reached for the reaction of Pt(acac)₂ and PVP in EG. The sample marked (*) is at the homogenization step at 100 °C.

To validate the color change observed in Fig S1-1 as an indicative parameter to the relative reaction kinetics of the nanoparticle precursor, high-resolution BF-SEM images were acquired on a Hitachi SU8230 to characterize the samples presented in Fig. S1-1. A small drop from each of the sample volumes was deposited onto a TEM-grid (Fig. S1-2).

SEM images for the sample at 100 °C (*) (Fig. S1-2) seem to show a few very small nanoparticles to be present, although they are scarce on the grid. The low number of particles and their small size makes it impossible to reliably measure their size. This indicates the nucleation process has barely started at these conditions. The finding from SEM corresponds well with the straw-yellow color of the reaction mixture at this time-point, which is identical to the color of the solution of the unreacted reactants before any heat was applied to the system.

Immediately after reaching 195 °C, corresponding to the sample “0 min” in Fig. S1-2, small nanoparticles ($4.80 \pm 0.80 \text{ nm}$) are clearly detected, and they grow larger throughout the progress of the reaction (5-50 min), with a final particle size of $7.27 \pm 0.93 \text{ nm}$. Some small fluctuations in the average particle size are observed in the measured averages with respect

to increasing reaction time, however the general trend is that the average particle size increases with reaction time. Although the method cannot distinguish between the formation of new nanoparticles and the growth of already existing nanoparticles, the change in color of the reaction mixture is at least correlated to these processes, and can thus be used as an indicative parameter for qualitatively evaluating the relative reaction kinetics of the metal precursors. As a side note, the dark color of the reaction mixture at the end of the reaction (50 min mark) matches perfectly with the color of the nanoparticles when they are redispersed after the nanoparticle washing procedure (see Experimental section).

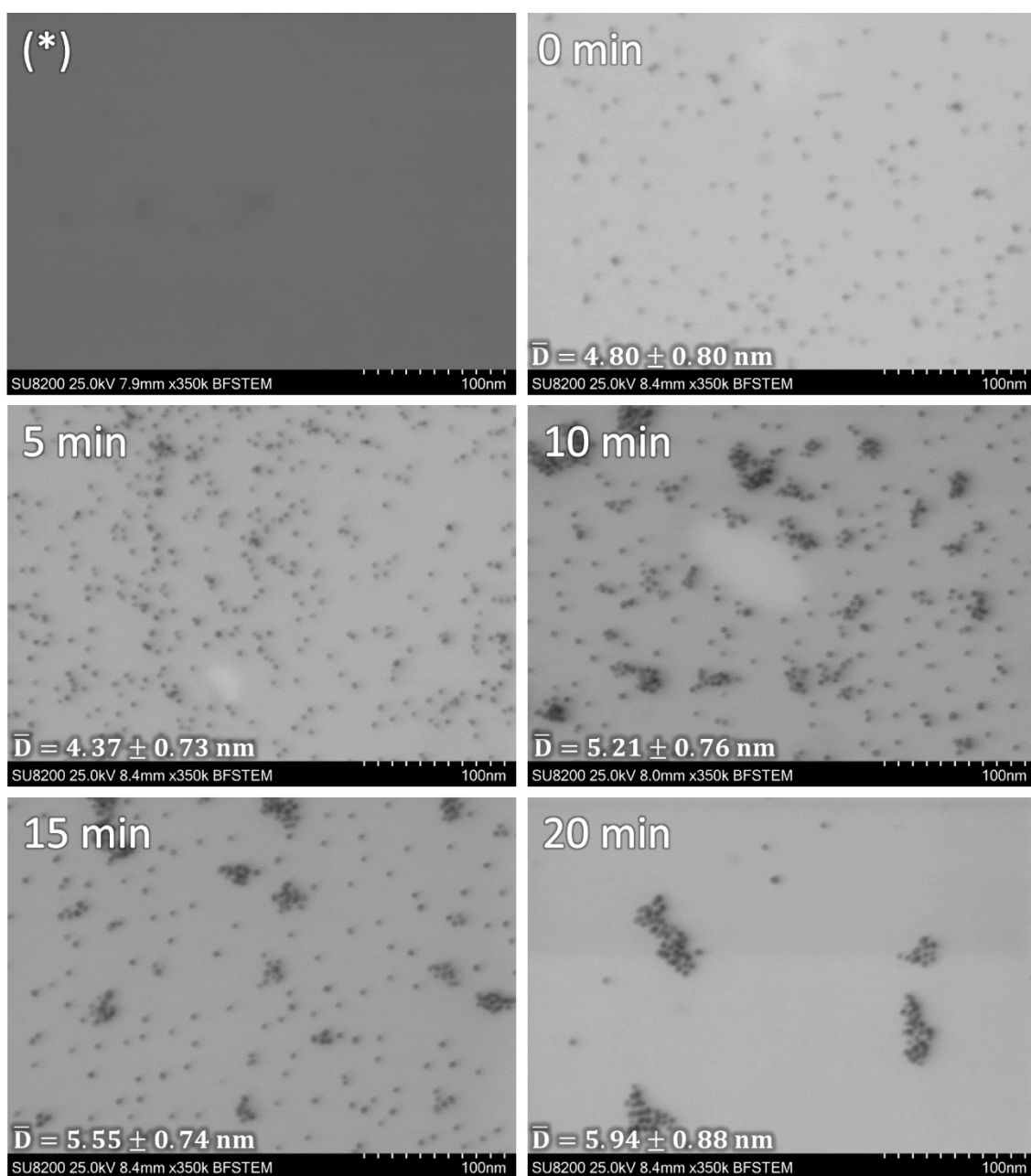


Fig. S1-2 High-resolution SEM images of the sample corresponding to the timepoints in Fig. S1-1.

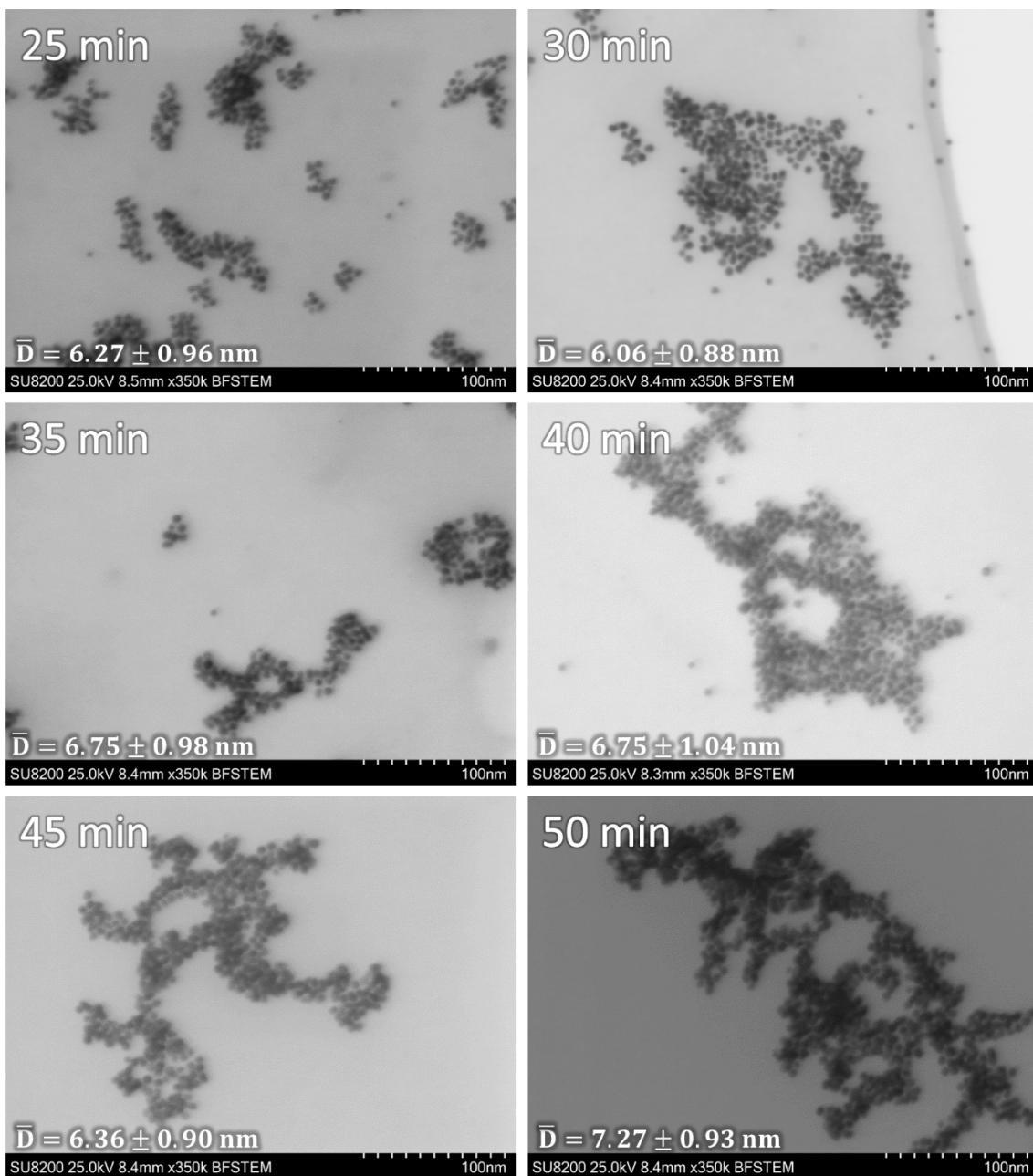
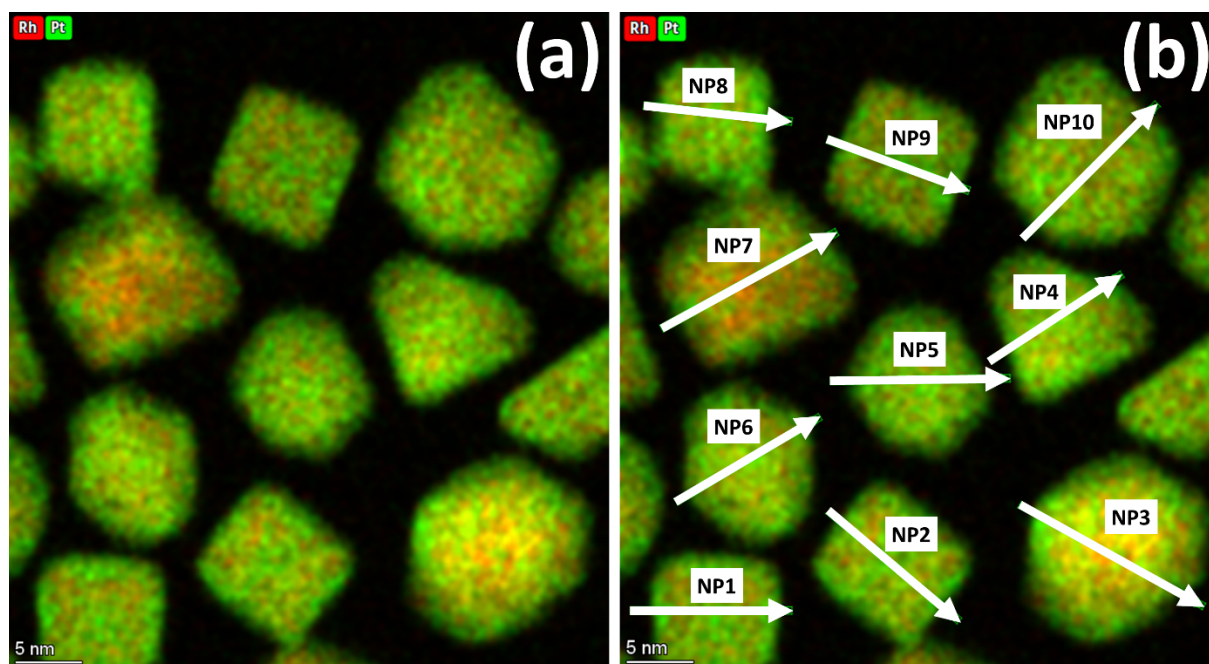


Fig. S1-2 High-resolution SEM images of the sample corresponding to the timepoints in Fig. S1-1.

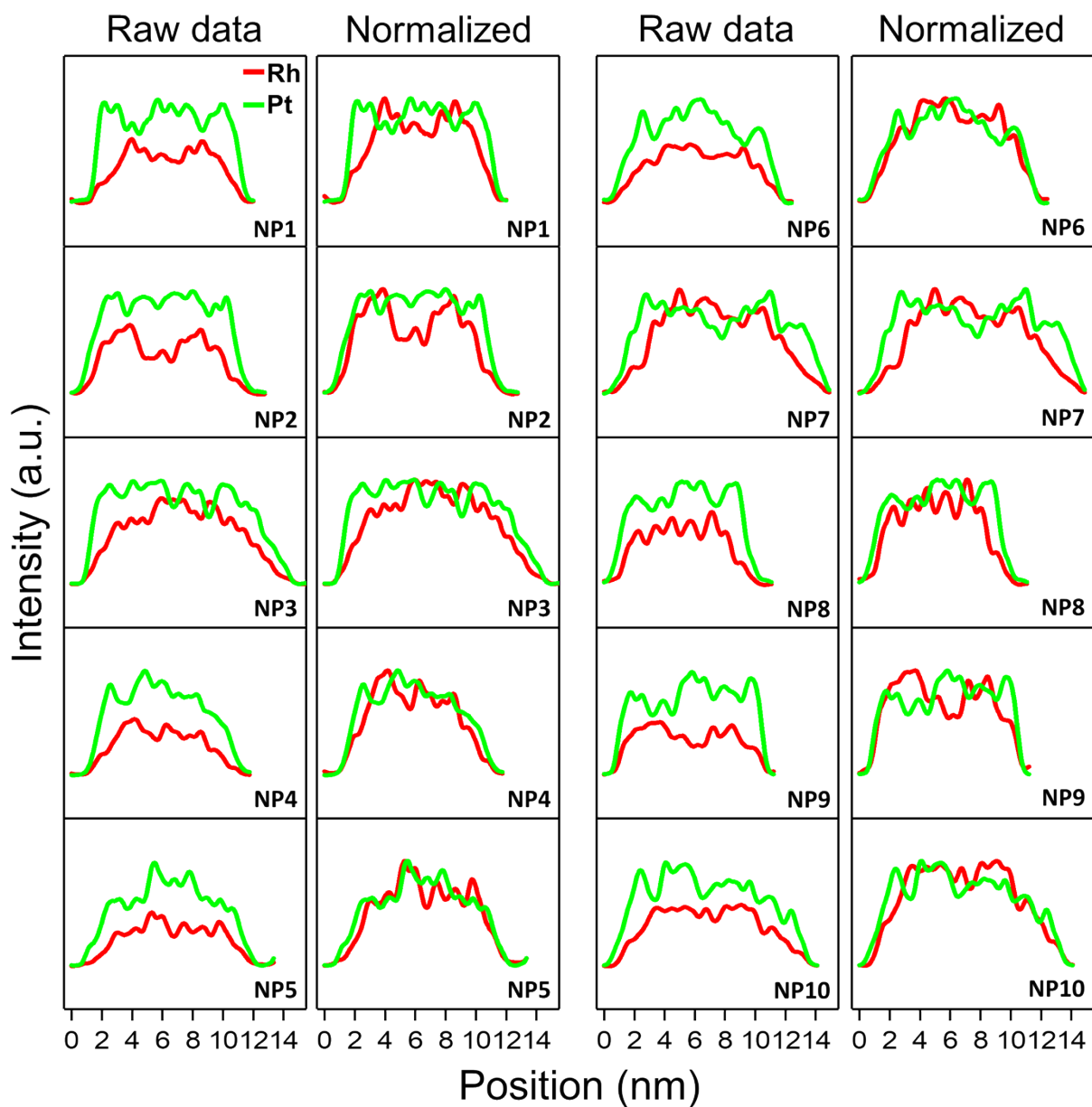
S2 Pt-Rh solid solution nanoparticles – the effect of prolonged reaction time

An experiment with a prolonged reaction time, surpassing the estimated end-point of the faster $\text{Rh}(\text{acac})_3$ precursor reaction window in Fig. 1d in the main manuscript, was performed. This was to verify that this would lead to the formation of a shell of the metal reduced from the slower reacting precursor ($\text{Pt}(\text{acac})_2$), and thus increase the relative amount of Pt in the nanoparticles. The nanoparticles were synthesized with molar precursor ratio of $\text{Pt}(\text{acac})_2:\text{Rh}(\text{acac})_3 = 3:1$ in ethylene glycol at 195°C with 120 min reaction time. EDS mapping (Fig. S2-1) and line scan analyses (Fig. S2-2) were recorded for 10 selected Pt-Rh solid solution nanoparticles together with an average large area (>1000 nanoparticles) spectrum (Fig. S2-3).

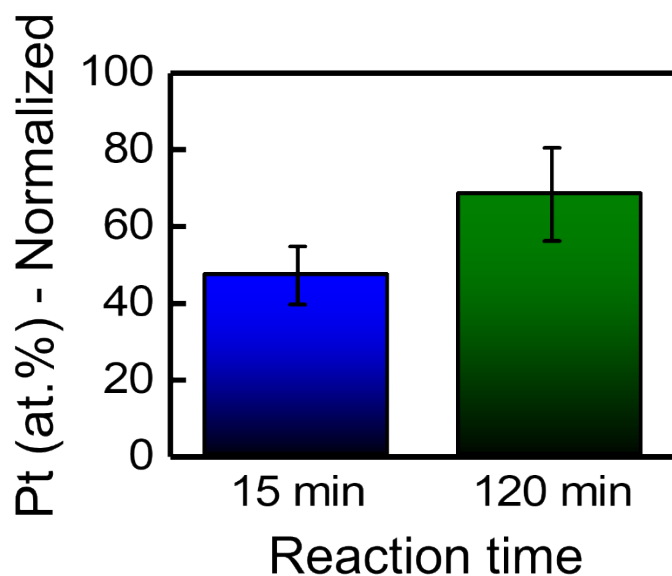
Based on the EDS elemental maps (Fig. S2-1), and corresponding line scans (Fig. S2-2), a thin Pt-rich shell can be seen on the Pt-Rh solid solution nanoparticles. To better visualize the distribution of Rh and Pt in the nanoparticles, the line scan intensities of each element were normalized to 1. The Pt-rich shell is most evident from the normalized EDS intensity line scans of NP1-4 and NP7-10. The large area average EDS spectra of >1000 nanoparticles (Fig. S2-3) shows that the longer reaction time of 120 minutes resulted in a significantly higher Pt content in the particles, compared to a reaction time of 15 minutes, which is in agreement with the line scan results.



S2-1 EDS elemental map (Rh in red, Pt in green) (a) with complementary EDS-background corrected intensity profile line scans (b) of 10 Pt-Rh solid solution nanoparticles (NP1-10) synthesized with a long reaction time (120 min). The results from the line scans are presented in Fig. S2-2.



S2-2 Intensity profile line scans results from NP1-10 of the Pt-Rh solid solution nanoparticles in Fig. S2-1. The figure shows raw EDS intensity (left) and Pt signal and Rh signal each normalized to 1.



S2-3 Large area (>1000 nanoparticles) quantitative EDS results from the two solid solution nanoparticle samples synthesized with molar precursor ratios of $\text{Pt}(\text{acac})_2:\text{Rh}(\text{acac})_3 = 3:1$ with 15 min (blue) and 120 min (green) reaction time. The y-axis shows the Pt composition (normalized to Pt and Rh). Note that the 15 min sample is the same data as presented in Fig. 3a, and is included here for comparison.

S3 Histograms of nanoparticle size distributions

Histograms to show the nanoparticle size distributions are shown in Fig. S3

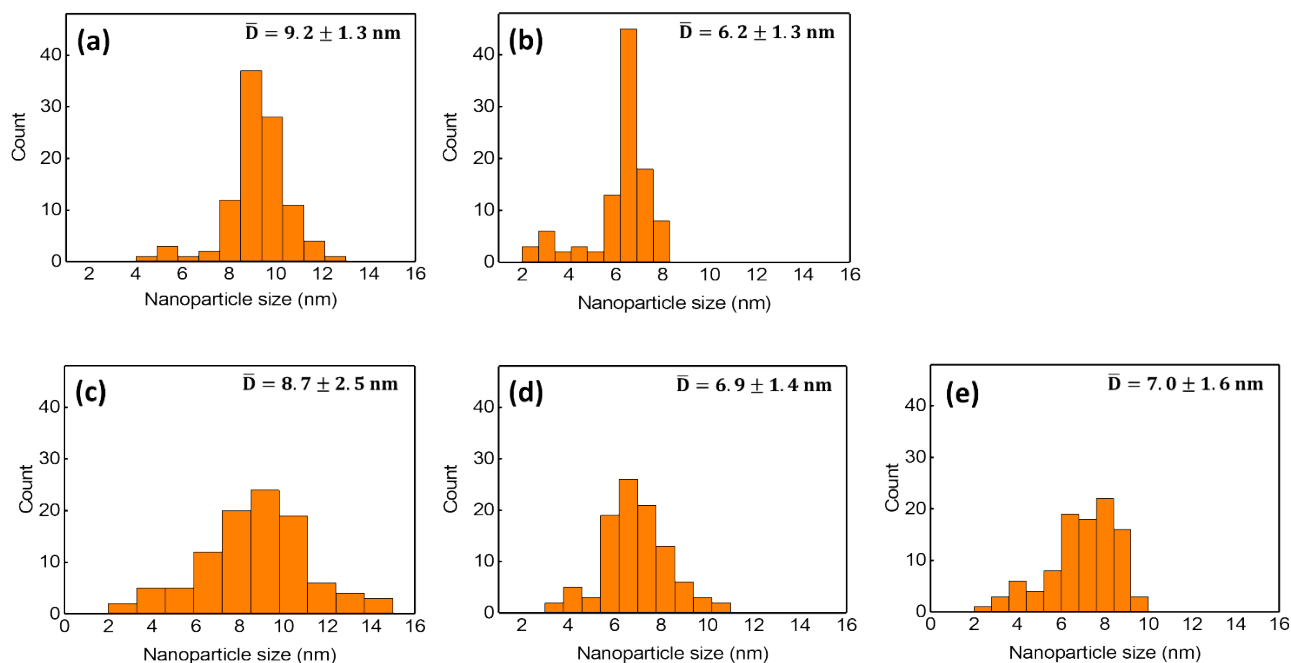
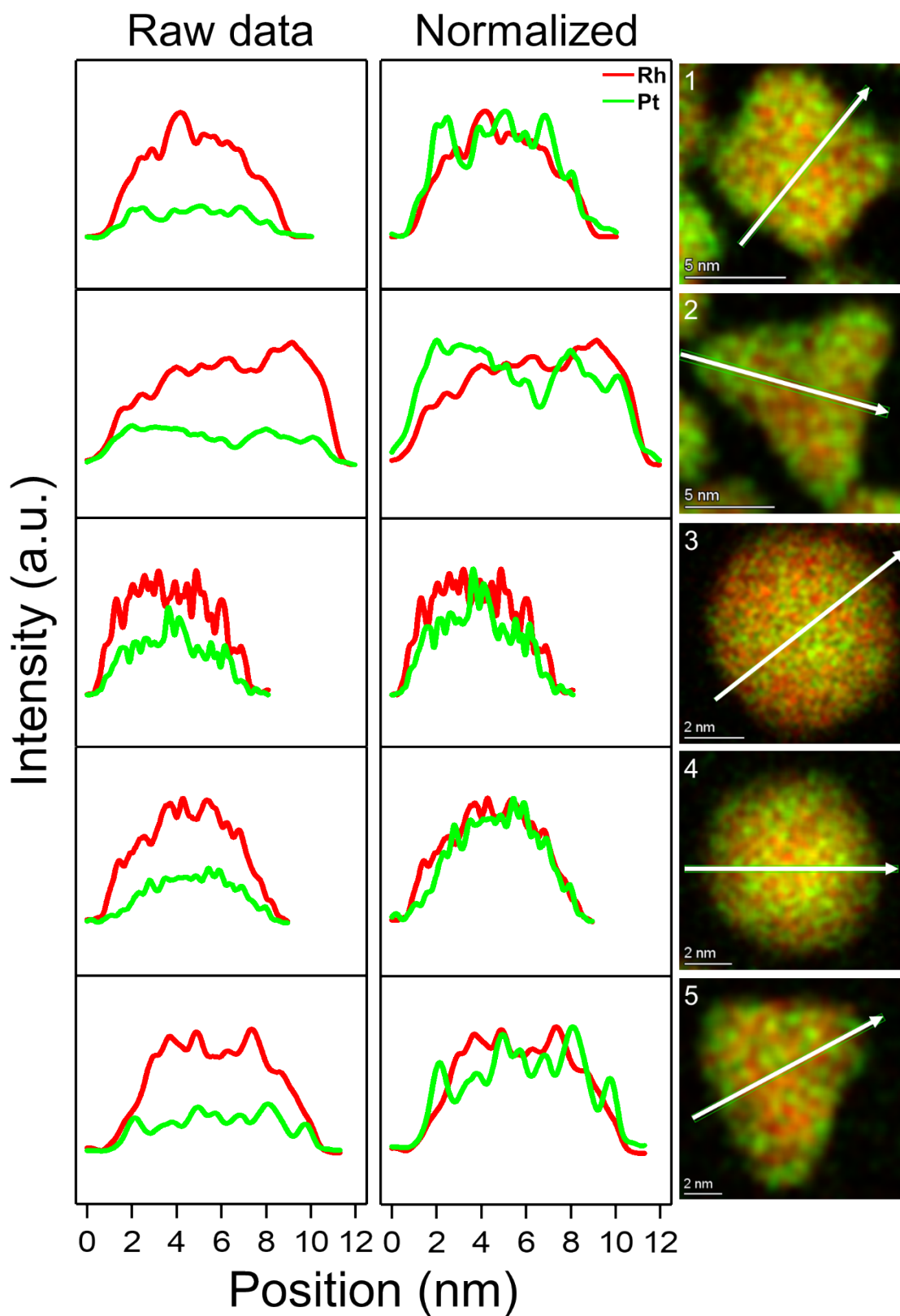


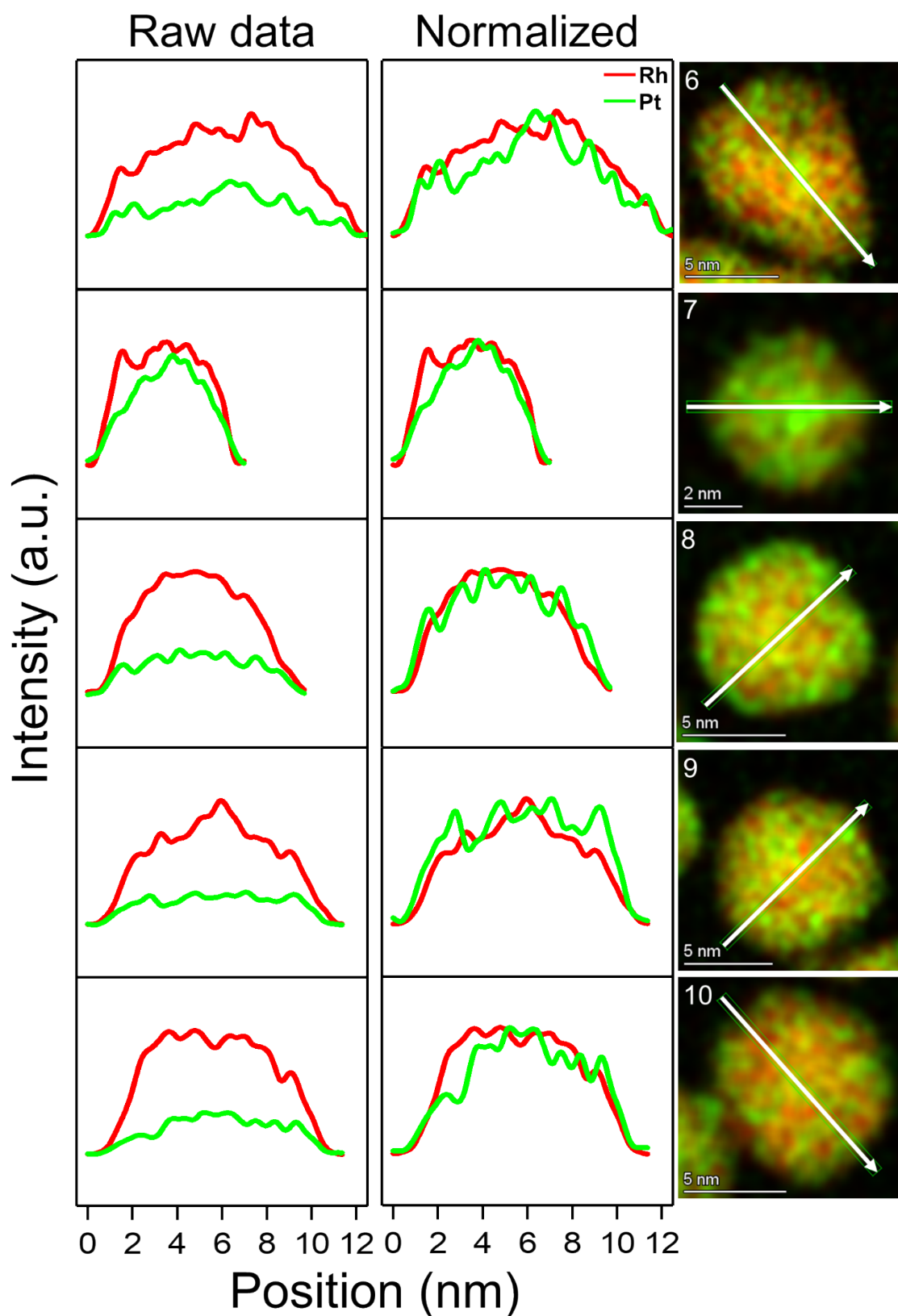
Fig. S3 Histograms showing the nanoparticle size distribution from the $\text{Rh}(\text{core})\text{-Pt}(\text{shell})$ sample (a), $\text{Pt}(\text{core})\text{-Rh}(\text{shell})$ sample centrifuged at low speed (1000 rpm, 5 min) (b), solid solution samples with molar precursor ratios of $\text{Pt}(\text{acac})_2 : \text{Rh}(\text{acac})_3$ of 1:1 (c), 3:1 (d), and 9:1 (e).

Histograms are based on 100 NPs as sample size.

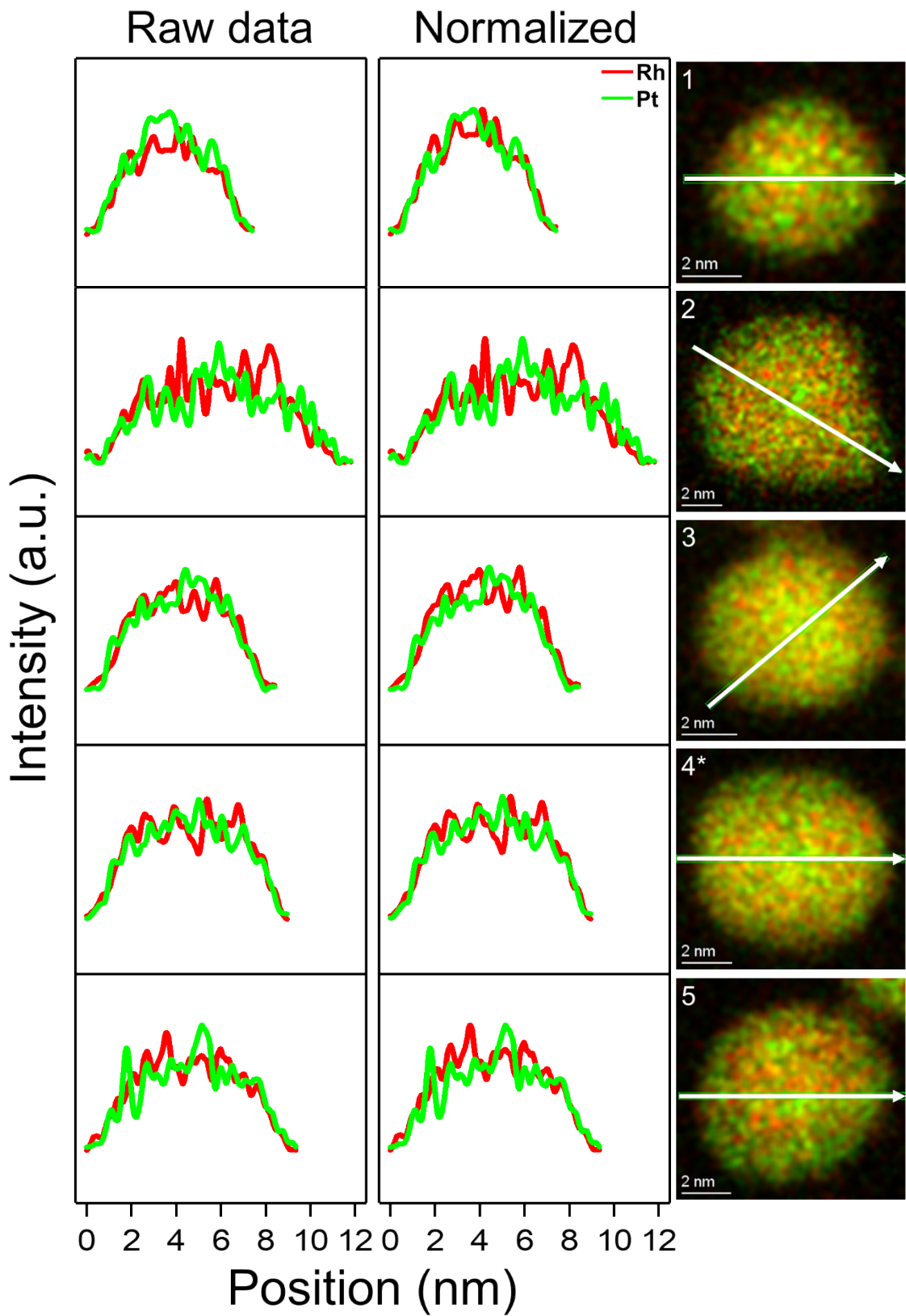
S4 Pt-Rh solid solution nanoparticles – energy dispersive X-ray spectroscopy line scans

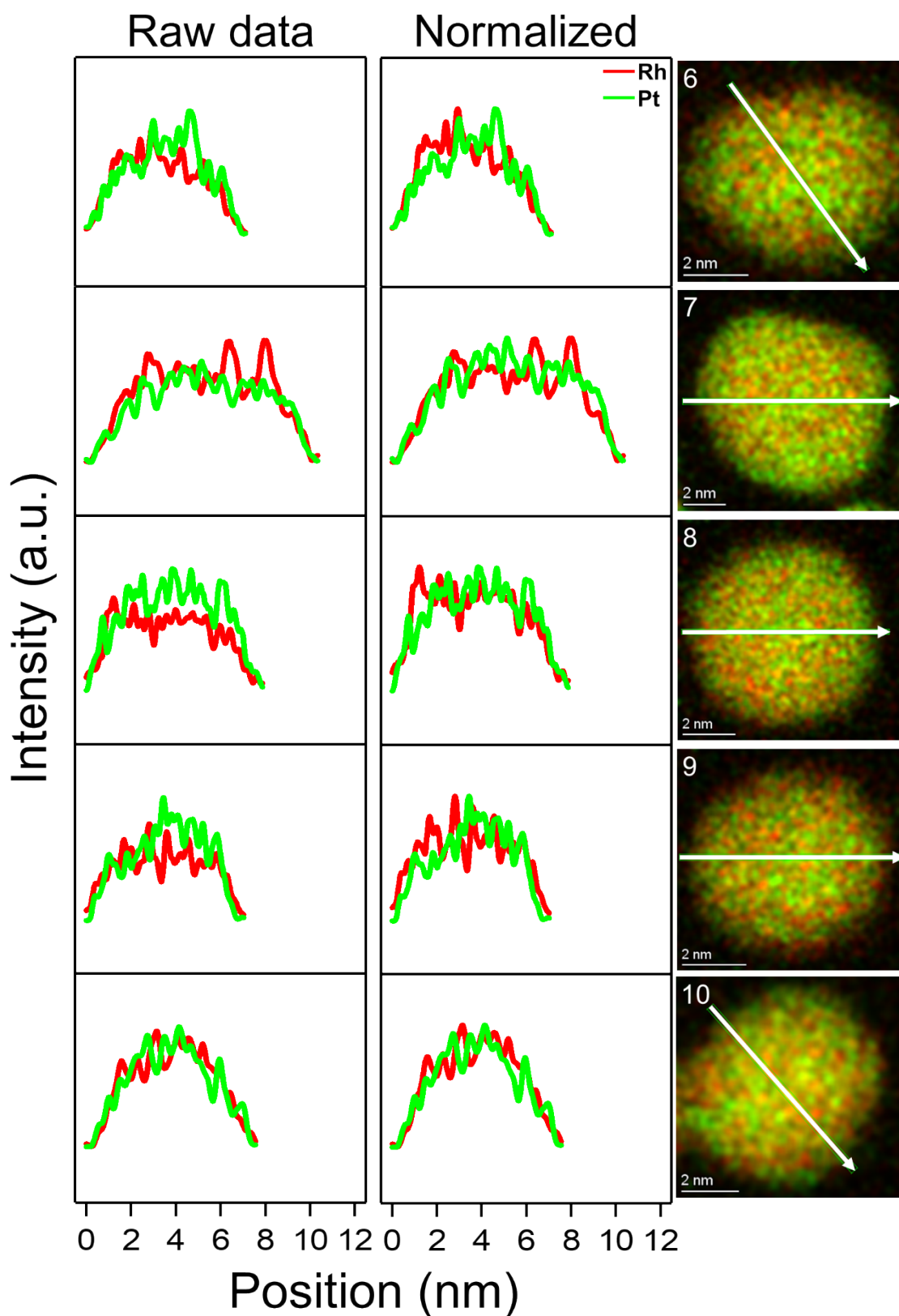
The EDS background-corrected Pt- and Rh line scan intensity profiles of the individual solid solution nanoparticles from the three samples synthesized with molar precursor ratios $\text{Pt}(\text{acac})_2:\text{Rh}(\text{acac})_3$ equal to 1:1, 3:1 and 9:1 are shown in Fig. S4. Since the Rh intensity largely follows that of the Pt intensity in the normalized line scans, we conclude the two elements are homogeneously distributed in the nanoparticles.



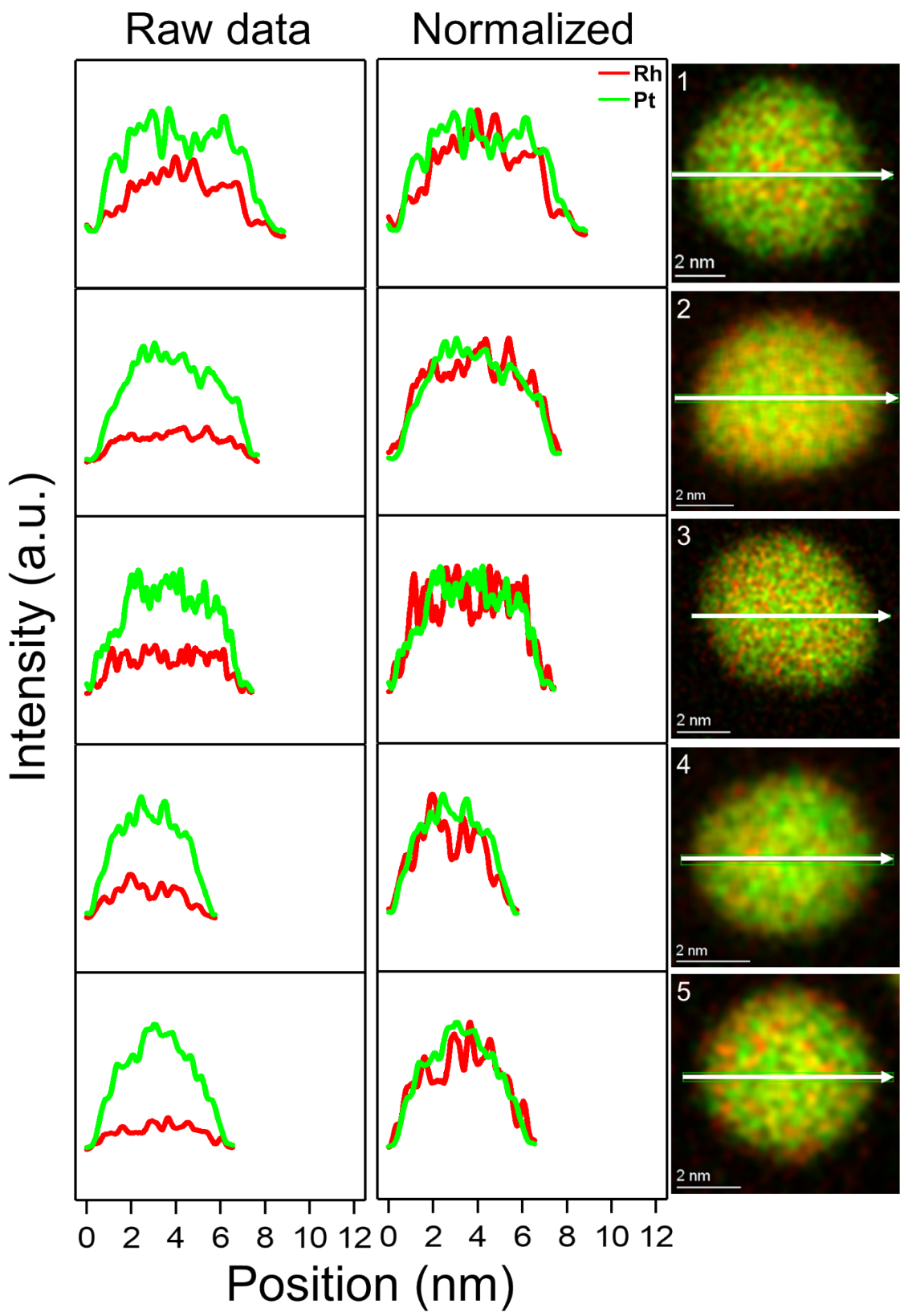


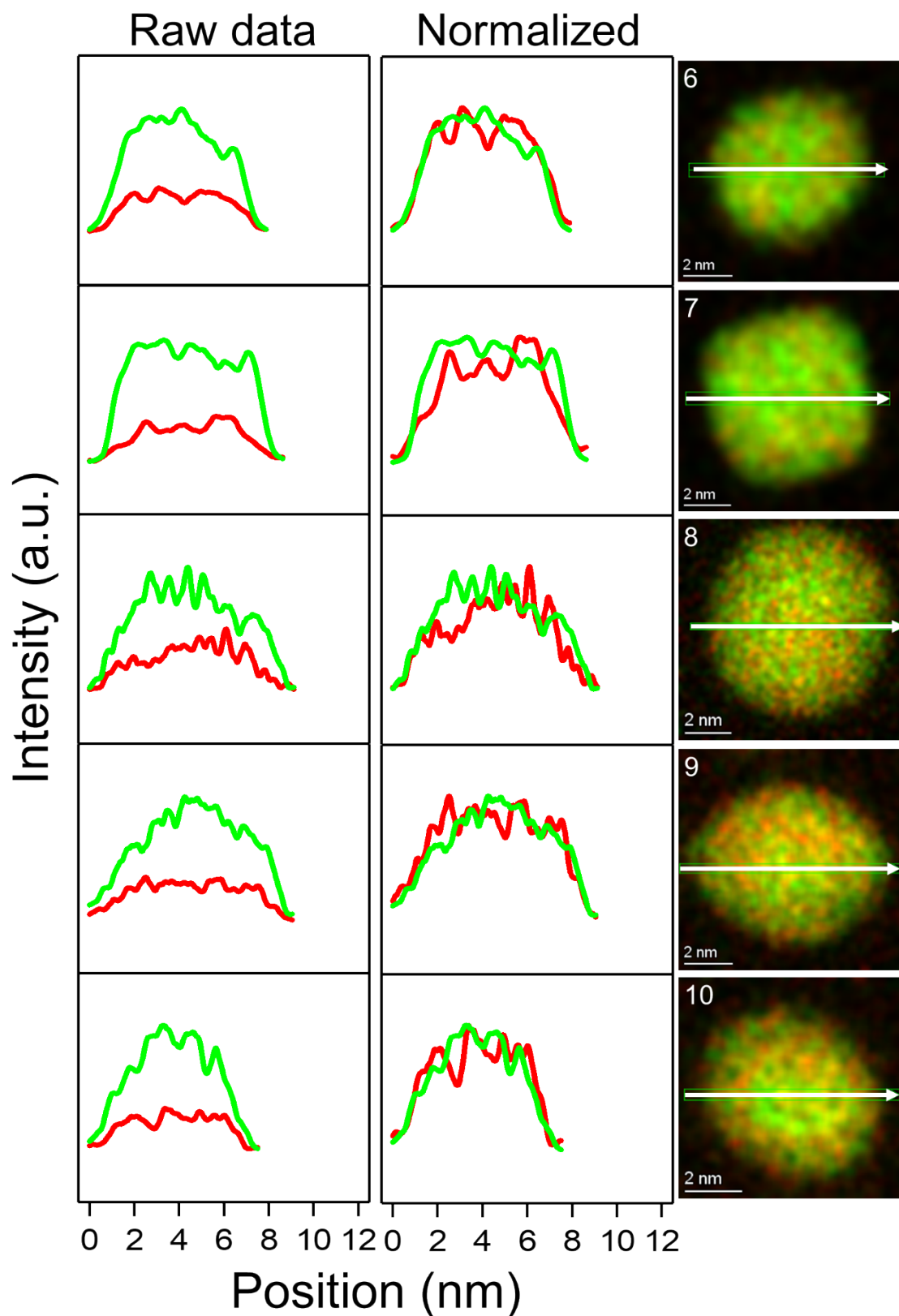
S4-1 EDS line scans and corresponding EDS elemental maps from 1-10 of the same nanoparticles shown in Fig. 3 in the main manuscript of the sample synthesized with molar precursor ratio of $\text{Pt}(\text{acac})_2:\text{Rh}(\text{acac})_3 = 1:1$.





S4-2 EDS line scans and corresponding EDS elemental maps from 1-10 of the same nanoparticles as in Fig. 3 in the main manuscript of the sample synthesized with molar precursor ratio of $\text{Pt}(\text{acac})_2:\text{Rh}(\text{acac})_3 = 3:1$. *The EDS map from nanoparticle “4” is the one reported in Fig. 1 in the main manuscript.





S4-3 EDS line scans and corresponding EDS elemental maps from 1-10 of the same nanoparticles shown in Fig. 3 in the main manuscript of the sample synthesized with molar precursor ratio of $\text{Pt}(\text{acac})_2:\text{Rh}(\text{acac})_3 = 9:1$.

S5 Stability Against Oxidation

Colloidal-solution-based nanoparticle synthesis is normally carried out under inert conditions (e.g. Ar flow) to ensure an oxygen-free environment, both due to the flammability of the solvent and to suppress oxygen incorporation into the metal/alloy. The latter argument applies in particular for very small nanoparticles. To investigate the stability of the nanoparticles towards oxidation during synthesis and storage, we therefore produced Rh nanoparticles via the same synthesis protocol as for the Rh(core) in the Rh(core)-Pt(shell) nanoparticles (as reported in Fig. 2e-f in the main manuscript). Rh was chosen for this experiment as it is more easily oxidized than Pt^{1,2}. The samples were synthesized under inert conditions and subsequently kept in ambient air for one week. HAADF-STEM imaging and PXRD were performed to investigate the samples (Fig. S5). Fig. S5a and b show PXRD and HAADF-STEM of Rh nanoparticles that have not been exposed to oxygen at all (neither during synthesis nor during sample preparation – prepared in an Ar glovebox and transferred to the TEM using a Gatan Double Tilt Vacuum Transfer Holder, Model 648; PXRD was measured (in air) immediately after transferring from the glove box). Fig. S5c and d show PXRD and HAADF-STEM of Rh nanoparticles that were exposed to air for one week at ambient conditions. Several nanoparticles were analyzed using HAADF-STEM for both samples, with representative images shown.

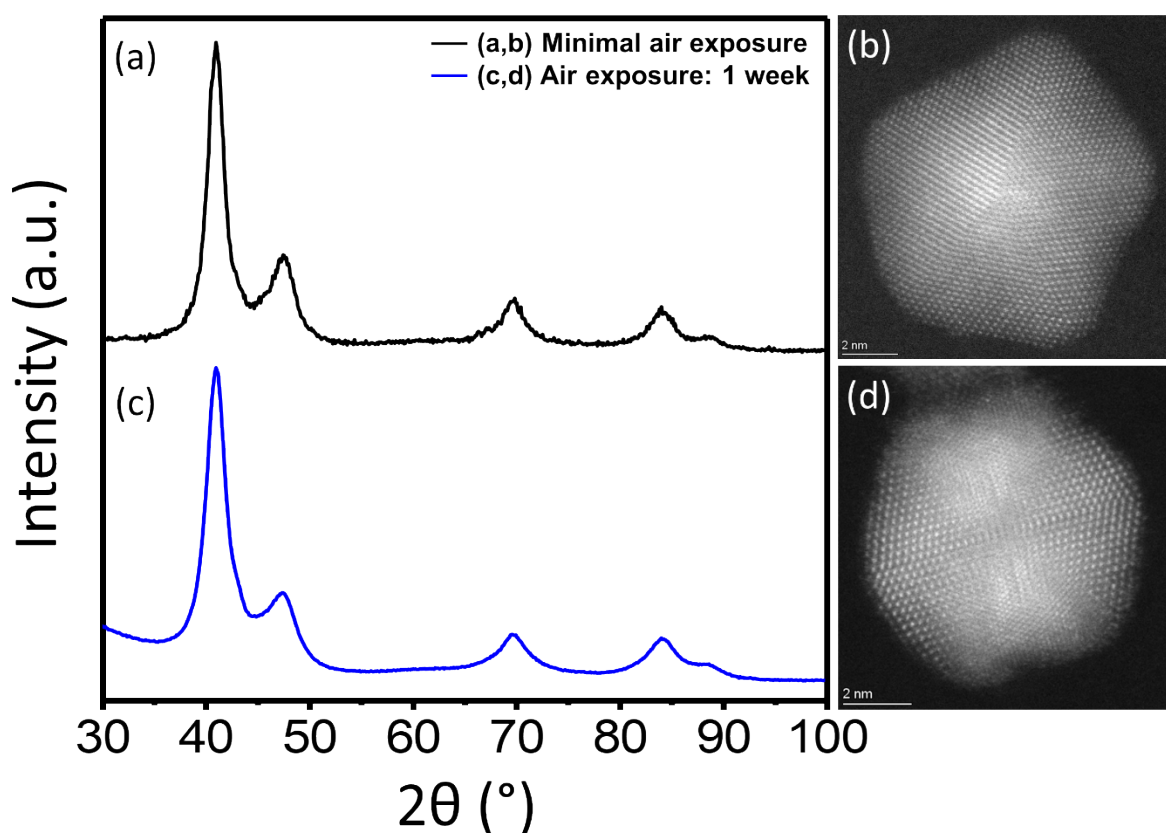


Fig. S5 Powder X-Ray Diffraction patterns and associated high-resolution HAADF-STEM images of Rh nanoparticles with two different post-treatments.

The PXRD data (Fig. S5a) of the non-oxygen exposed sample show solely Bragg reflections in accordance with bulk metallic ccp Rh (Crystallography Open Database ID: 9008482). Close inspection of the HAADF-STEM image of the sample (Fig. S5b) shows no signs of roughness in the outer rim of the particle, and no shell of lower brightness can be observed. These Rh nanoparticles are purely metallic. In the sample that was exposed to air for one week, the HAADF-STEM image may indicate minor oxide formation at the surface (Fig. S5d), although this is not conclusive, and it is not detectable in the corresponding diffraction pattern (Fig. S5c). These results confirm the Rh nanoparticles are quite stable when exposed to air at ambient temperature.

In conclusion, the inert handling allows us to provide oxygen-free nanoparticles, which is important when these are used as seeds in our core-shell nanoparticle synthesis.

S6 Rh(core)-Pt(shell) and Pt(core)-Rh(shell) Nanoparticles – Sample Homogeneity

An extended EDS analysis to show the homogeneity of the Rh(core)-Pt(shell) and Pt(core)-Rh(shell) samples was performed. The EDS maps (Fig. S6 and S7) are taken to be representative of the sample as they were collected from areas far apart from each other on the TEM grid. For the Pt(core)-Rh(shell) sample, EDS maps of individual nanoparticles were captured because the Rh shell was very thin, requiring higher zoom to obtain acceptable maps.

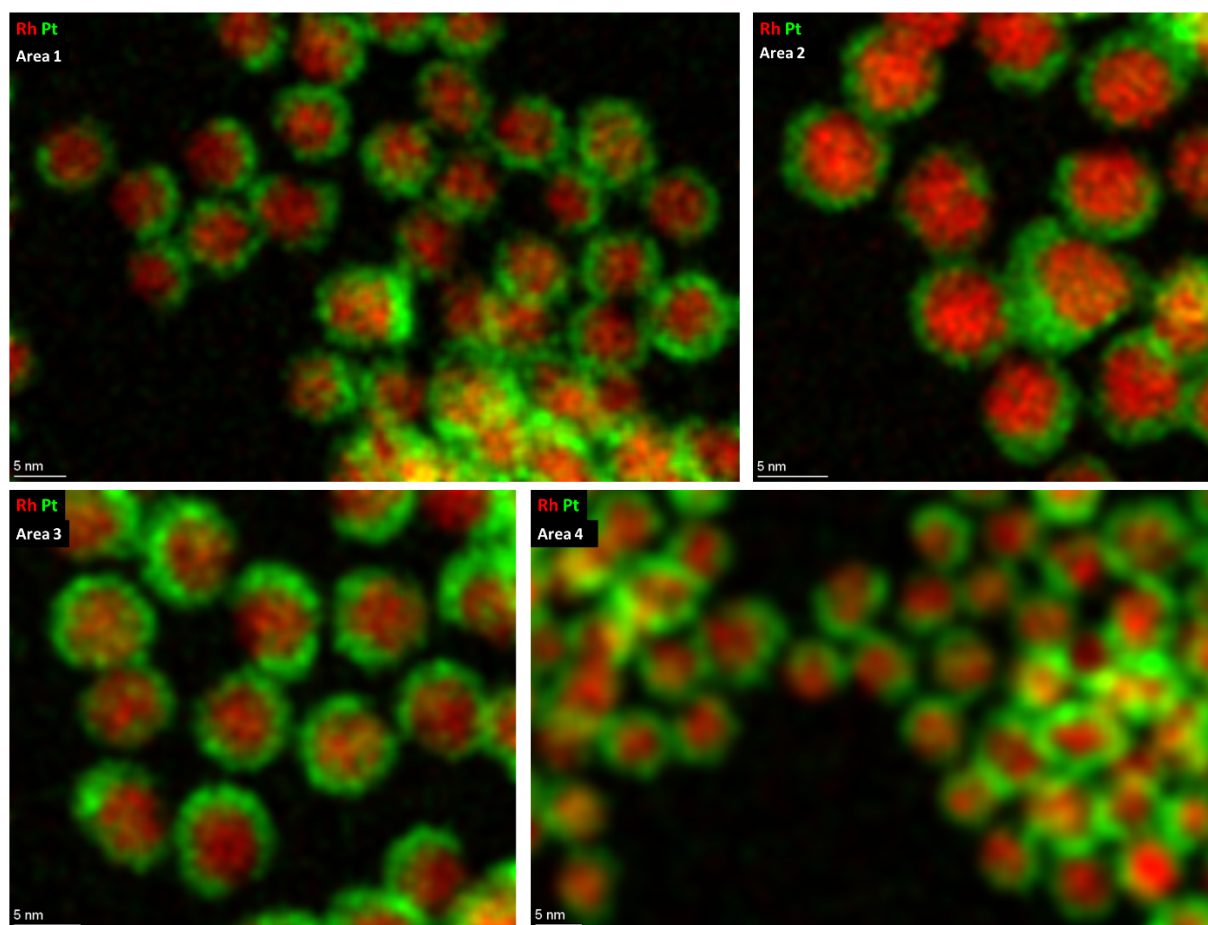


Fig. S6 EDS elemental maps (Rh in red, Pt in green) of Rh(core)-Pt(shell) nanoparticles.

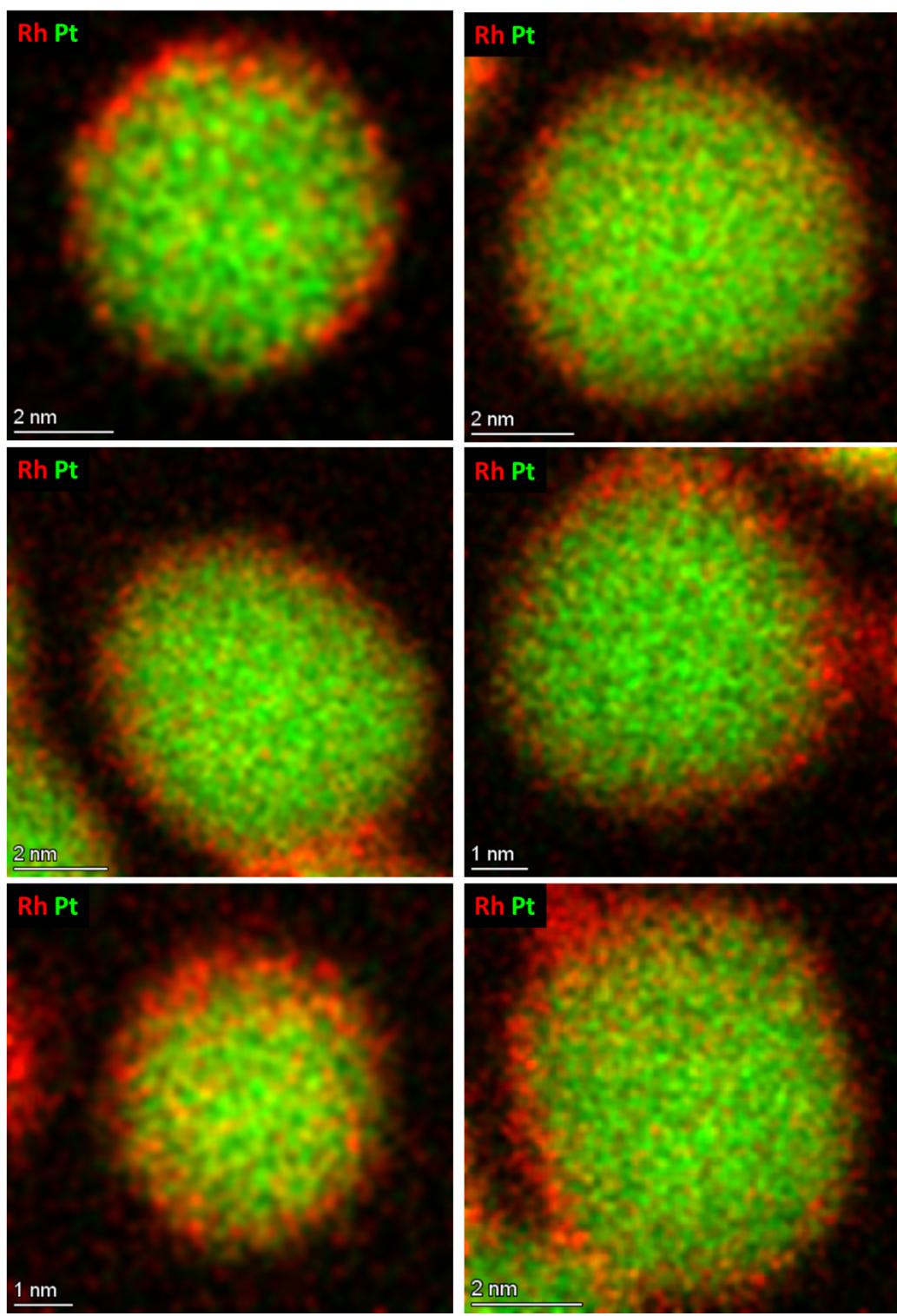


Fig. S7 EDS elemental maps (Rh in red, Pt in green) of Pt(core)-Rh(shell) nanoparticles.

Overview BF-STEM images of the Pt(core)-Rh(shell) sample that has been purified by centrifugation at lower speed (1000 rpm for 5 minutes) are captured far apart on the TEM grid to show representative sample homogeneity, and are presented in figure S8.

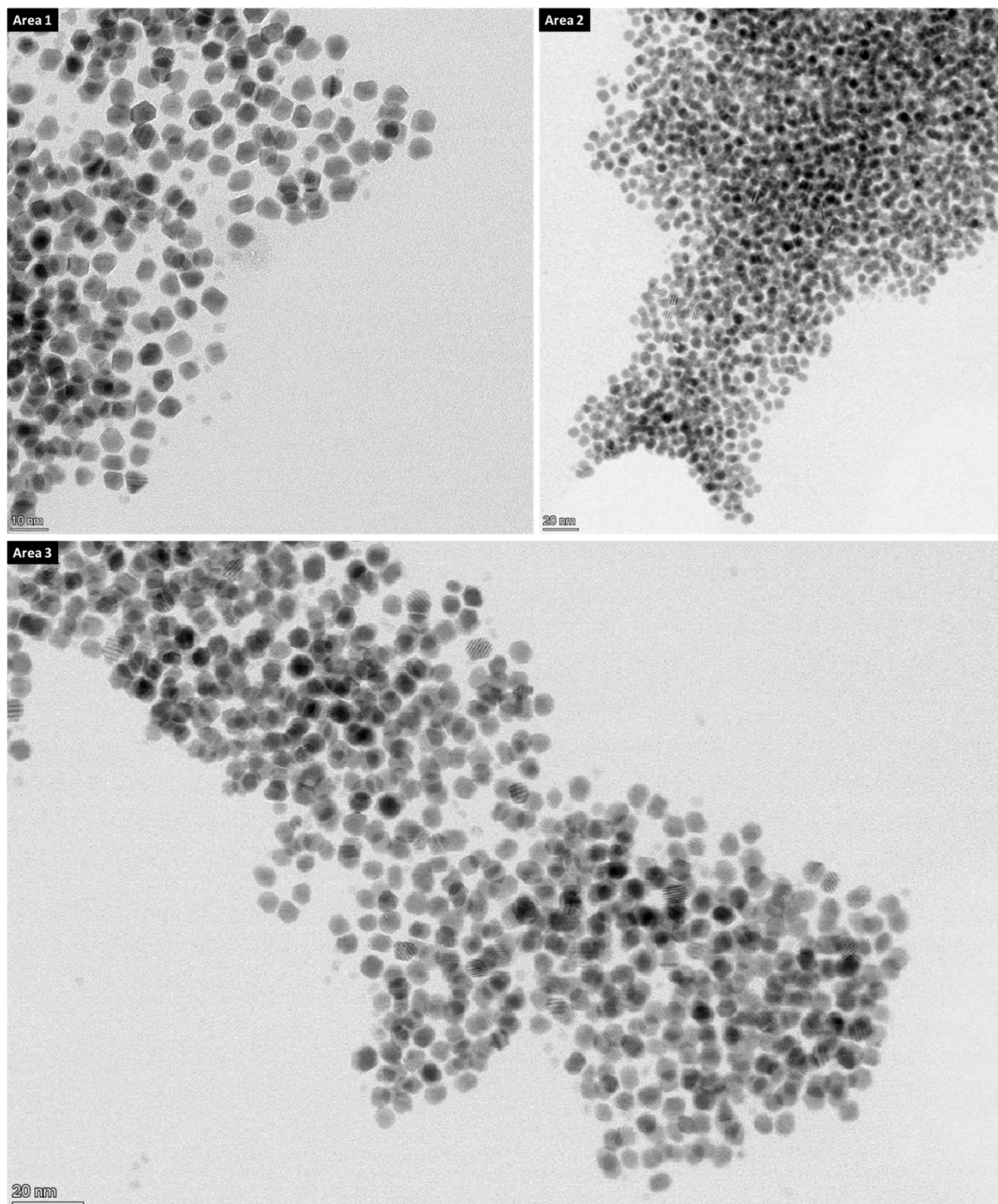


Fig. S7 BF-STEM overview images of the Pt(core)-Rh(shell) sample centrifuged at low speed (1000 rpm for 5 minutes).

Bibliographic references

1. O. Ivashenko, N. Johansson, C. Pettersen, M. Jensen, J. Zheng, J. Schnadt and A. O. Sjøstad, *ACS Catalysis*, 2021, **11**, 8261-8273.
2. S. D. Miller, N. İnoğlu and J. R. Kitchin, *The Journal of Chemical Physics*, 2011, **134**, 104709.